Received: 27 July 2022 | Revised: 4 October 2022 | Accepted: 7 October 2022

DOI: 10.1002/mmce.23498

ORIGINAL ARTICLE

INTERNATIONAL JOURNAL OF RF AND MICROWAVE COMPUTER-AIDED ENGINEERING WILEY

Co-design of a low noise amplifier with compact substrate integrated waveguide bandpass filtering matching network

Phanam Pech[1] | **Phirun Kim**[2,3] | **Yongchae Jeong**[1]

[1]Division of Electronics and Information Engineering, Jeonbuk National University, Jeonju-si, Jeollabuk-do, Republic of Korea

[2]Department of Frequency Spectrum Management, Ministry of Posts and Telecommunication of Cambodia, Phnom Penh, Cambodia

[3]Institute of Digital and Innovation, Cambodia Academy of Digital Technology, Phnom Penh, Cambodia

Correspondence
Yongchae Jeong, Division of Electronics and Information Engineering, Jeonbuk National University, Jeonju-si, Jeollabuk-do, 54896, Republic of Korea.
Email: ycjeong@jbnu.ac.kr

Funding information
National Research Foundation (NRF) of Korea Grant funded by Korea Government (MSIT), under Grant 2020R1A2C2012057 and in part by Basic Science Research Program through the NRF of Korea, funded by Ministry of Education, under Grant, Grant/Award Number: 2019R1A6A1A09031717

Abstract

This article presents a co-design of a low noise amplifier (LNA) and bandpass filter (BPF) input matching network (IMN) based on quarter-mode and one-eight-mode substrate integrated waveguide (SIW) cavities. The transmission zeros (TZs) of the proposed BPF IMN occur in the stopband and demonstrate improved frequency selectivity compared to conventional methods. Our design can reduce the complexity and circuit sizes of receiving BPFs and LNAs in communication systems, and improve the receiving performance of radio frequency (RF) front-end circuitry. Three different LNAs were fabricated and tested. The proposed LNA features a three-stage compact-size SIW BPF IMN at a center frequency (f_0) of 8 GHz. The proposed LNA with a compact SIW BPF IMN exhibits better electrical performance than a conventional LNA (CLNA) with a full-mode (FM) SIW BPF. We found that the small signal gains at f_0 of the standalone CLNA, FM SIW BPF cascaded with CLNA, and the proposed LNA were 15.69, 14.72, and 15.18 dB, respectively. The measured noise figure (NF) at f_0 of CLNA was 0.86 dB, while the NF of the FM SIW BPF cascaded with CLNA was 2.23 dB, and the NF of the proposed LNA at f_0 was 1.71 dB. In addition, the circuit size of the proposed LNA is 48% smaller than that of an FM SIW BPF cascaded with CLNA.

KEYWORDS

bandpass filter, low noise amplifier, one-eighth-mode cavity, quarter-mode cavity, substrate integrated waveguide

1 | INTRODUCTION

The development of modern communications and radar systems has increased the demand for power amplifiers (PAs), low noise amplifiers (LNAs), and bandpass filters (BPFs) that are compact, high quality, and easy to fabricate. Figure 1A shows the conventional radio frequency (RF) receiver of a wireless communications system.[1] If the BPF can directly match either the source (Z_S) and load (Z_L) impedances of a low noise transistor (LNT), or the input impedance of the antenna, then the overall circuit size, insertion loss, cost, and complexity of RF receiver systems can be reduced as can be seen in Figure 1B. Recent studies have reported the co-designs of waveguide BPFs and amplifiers based on coupling matrix. In References 2, 3, the authors designed matching networks (MNs) using conventional coupled waveguide cavities while the other parts of the amplifier were fabricated with a microstrip line (ML). In Reference 4, the authors used an active coupling matrix technique to

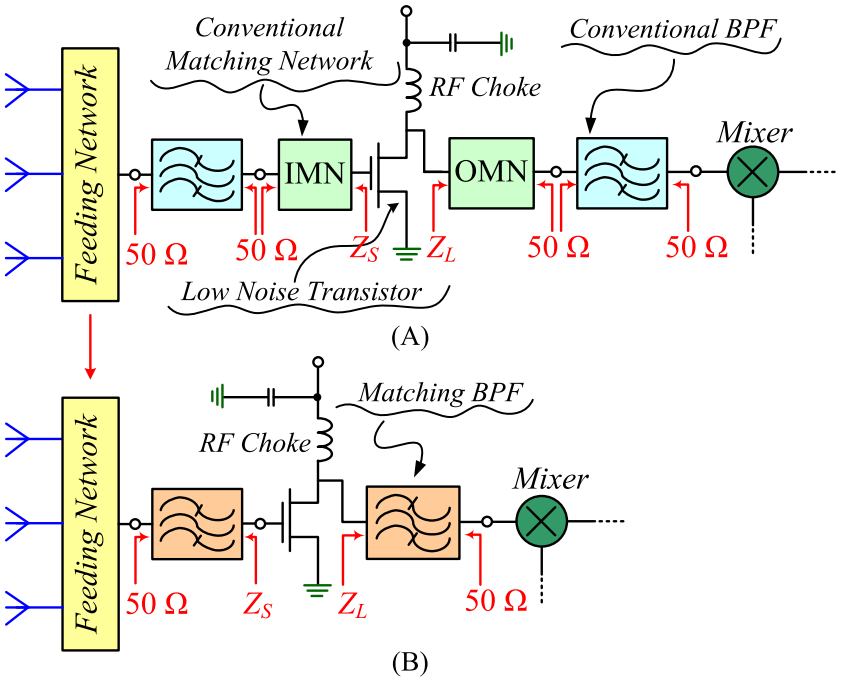

FIGURE 1 RF receiver of a typical wireless system with (A) the conventional matching networks and BPFs, and (B) a design that integrates BPFs and LNA

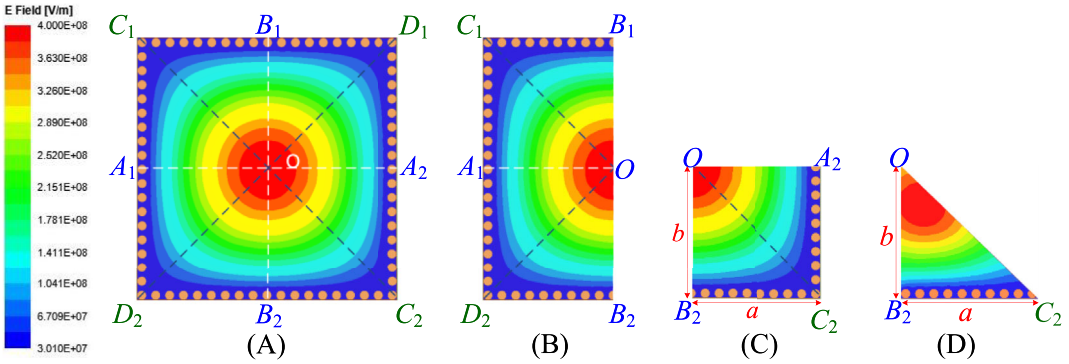

FIGURE 2 Electric field distribution of differently sized SIW cavities: (A) FM, (B) HM, (C) QM, and (D) OEM

design a substrate integrated waveguide (SIW) BPF and amplifier. Similarly, the integration design of microwave amplifier with SIW output matching network was presented in Reference 5. In References 4, 5, the MNs utilized full-modes (FM) SIW cavities. Despite the analysis and design methods in these works being wisely presented, however, these BPF MNs are large in size and are unable to be miniaturized in the volume of the whole system. In addition, difficulties in the fabrication process and the transition from waveguide to ML cannot be easily overcome.

The SIW has attracted considerable attention due to its high power-handling capability, *Q*-factor, low insertion loss, low cost, and ease of fabrication.[6–8] However, an FM SIW cavity occupies a relatively large area, especially in the microwave frequency range. To reduce the size of FM SIW cavities, half-mode (HM),[9–12] quarter-mode (QM),[13–16] and one-eighth-mode (OEM)[17–20] SIW cavities have been investigated.

Figure 2 shows the electric field distribution in differently-sized SIW cavities. An HM SIW is ∼50% of the size of an FM SIW cavity, as it is fabricated by bisecting an FM SIW cavity along its center plane. A QM SIW cavity is obtained by bisecting an FM SIW cavity twice along the equivalent magnetic wall, resulting in a size reduction of around 75%. Similarly, an OEM SIW cavity is produced by cutting the magnetic wall of the FM SIW cavity four times, resulting in a size reduction of around 87.5%. These cavities can support the same resonant frequency of the fundamental mode. In Reference 21, a compact and wide stopband SIW BPF using QM and OEM SIW cavities was presented. Transmission zeros (TZs) were observed in the stopband with high-frequency selectivity. However, in these studies, HM, QM, and OEM cavities were applied in the BPFs with equal termination impedances of 50-to-50 Ω. Moreover, the compact SIW BPF using difference mode cavities with arbitrary termination

impedances and the integrated design with the other circuits have not been presented up to date.

In this article, a new design integrating a compact SIW BPF with an LNA is presented. The SIW BPF is also operated as the input matching network (IMN) of LNA. The proposed compact SIW BPF was developed by mixing QM and OEM cavities mainly for size reduction and ease of fabrication. Three different LNAs were designed and fabricated and then evaluated based on electrical performance and circuit size. The proposed LNA with a compact SIW BPF IMN demonstrates better electrical performance, a reduced circuit size (around 48%), and a simpler design than an FM SIW BPF featuring a conventional LNA (CLNA).

2 | COMPLEX TERMINATION IMPEDANCES MIXED-MODE SIWS BPF DESIGN

As mentioned in Reference 5, complex termination impedance cannot be matched to an adjacent admittance inverter in general BPF designs. To address this issue, the resonant frequency of the resonator, located near the adjacent admittance inverter, must be detuned to match the reactive component of the termination impedance. According to the complex reactance, the detuned frequency can be determined using the following equation:[22]

$$f_{S1,Ln} = f_0\left[\sqrt{1+\left(\frac{X_{S,L}\mathrm{FBW}}{2R_{S,L}g_{0,n}g_{1,n+1}}\right)^2}+\frac{X_{S,L}\mathrm{FBW}}{2R_{S,L}g_{0,n}g_{1,n+1}}\right], \tag{1}$$

where $R_{S,L}$ and $X_{S,L}$ are the real and imaginary parts of the source and load impedances, respectively, g_0, g_1, g_n, and g_{n+1} are the element values of the low-pass prototype, $f_{S1,Ln}$ are the resonant frequencies of the different SIW cavities modes ($f_{r\_QM,OEM}$) which act as the first or last resonators. The assumption values of $f_{S1,Ln} = f_{r\_QM,OEM}$ are used to estimate the edge lengths of the cavities. The resonant frequency of intermediate resonators is not altered by complex termination impedances.

As shown in Figure 2C, the QM SIW cavity has two metallic walls and two open sides. Therefore, the QM SIW cavity can be located at the first, intermediate, and last stages of the BPF. By properly bisecting the QM SIW cavity, OEM SIW cavities may be obtained with the same edge lengths, a and b, as a QM SIW (Figure 2D). As the OEM SIW cavity has one metallic wall and two open sides, it should be placed at the first and/or last stages of the BPF. The resonant frequencies of QM and OEM SIW cavities can be estimated using the following equation:[20]

$$f_{r\_QM,OEM} = \frac{c}{2\pi\sqrt{\mu_r\varepsilon_r}}\left[\sqrt{\left(\frac{3.14}{a_{\mathrm{eff}}}\right)^2+\left(\frac{3.14}{b_{\mathrm{eff}}}\right)^2}\right] \tag{2}$$

$$a = a_{eff}+\frac{d^2}{0.95p}-\Delta w \tag{3a}$$

$$b = b_{eff}+\frac{d^2}{0.95p}-\Delta w \tag{3b}$$

$$\Delta w = h\left[\left(0.05+\frac{0.3}{\varepsilon_r}\right)\times\ln\left(0.79\frac{a_{eff}}{h^3}+\frac{104\left(a_{eff}/2\right)-261}{h^2}+\frac{38}{h}+2.77\right)\right], \tag{3c}$$

where c is the velocity of light in a vacuum, μ_r and ε_r are the relative permeability and permittivity of the substrate, respectively, a_{eff} and b_{eff} are the edge lengths of the equivalent resonant cavity, h represents the thickness of the substrate, d is the diameter of the metalized via, p is the pitch between adjacent via holes. Δw is the additional width that accounts for the effect of the fringing fields on the equivalent magnetic walls. Δw is functions of a_{eff}, h, and ε_r.

The QM and OEM SIW cavities feature two open sides that do not form a perfect magnetic wall, causing magnetism to leak, which leads to a lower quality factor (Q) than that of FM SIW cavities. Due to a decreased Q value, QM and OEM SIW cavities may not be applicable in the design of high-Q BPFs with narrow bandwidth. However, as a strong coupling coefficient between two different SIW cavity modes ($K_{i,i+1}$) can be easily obtained, QM and OEM SIW cavities can be used in broadband BPFs which the FM SIW cavity cannot easily provide. The subscript i represents the order of the SIW resonator. External quality factors ($Q_{eS,eL}$) and $K_{i,i+1}$ are very important parameters in the design of BPFS. $Q_{eS,eL}$ can be calculated using Equation (4), while $K_{i,i+1}$ can be calculated using Equation (5).[23]

$$Q_{eS,eL} = \frac{g_{0,n}g_{1,n+1}}{\mathrm{FBW}}, \tag{4}$$

$$K_{i,i+1} = \frac{\mathrm{FBW}}{\sqrt{g_i g_{i+1}}}, \quad i = 1, 2, \ldots, n, \tag{5}$$

$Q_{eS,eL}$ and $K_{i,i+1}$ values can be obtained from electromagnetic (EM) simulation by using the following equation:

$$Q_{eS\_EM,eL\_EM} = \frac{f_{S1,Ln}}{\Delta f_{\pm 3\mathrm{dB}}} \tag{6}$$

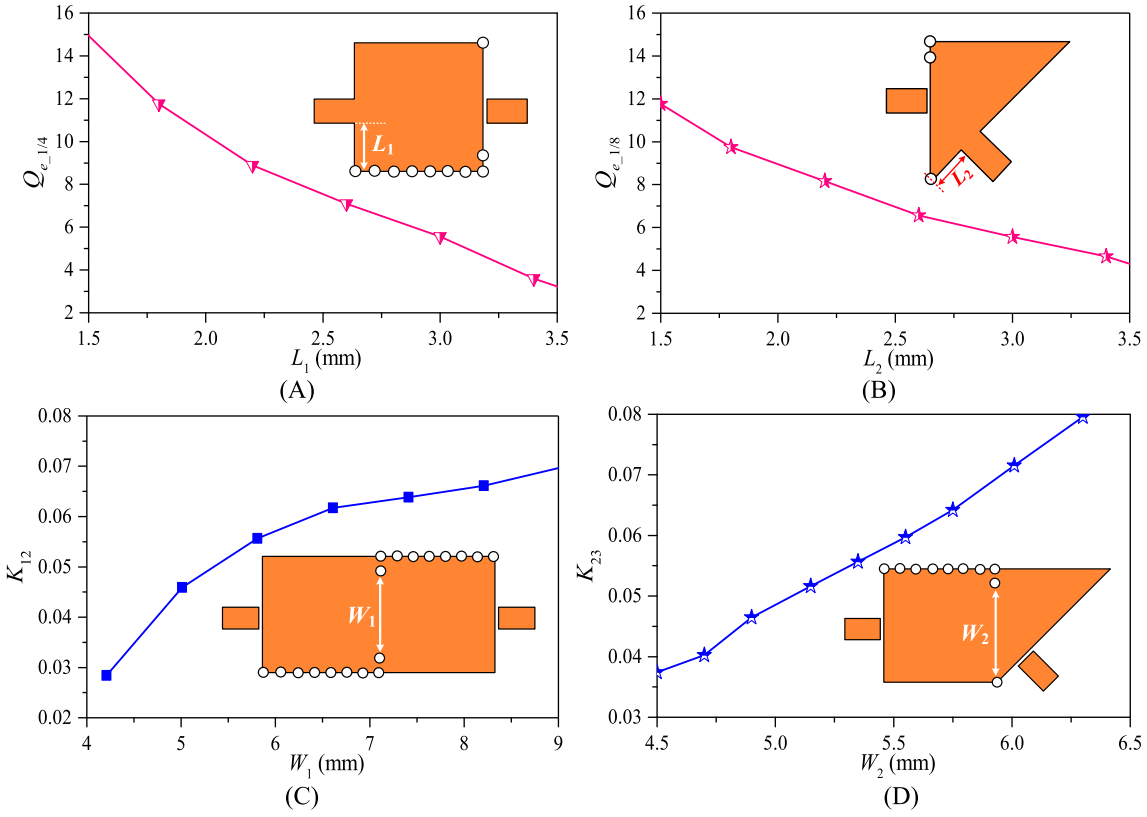

FIGURE 3 (A) $Q_{eS,eL}$ of QM SIW cavity according to L_1, (B) $Q_{eS,eL}$ of OEM SIW cavity according to L_2, (C) K_{12} of QM/QM SIW cavities according to W_1, and (D) K_{23} of QM/OEM SIW cavities according to W_2

$$K_{i,i+1} = \pm \frac{f_H^2 - f_L^2}{f_H^2 + f_L^2}, \tag{7}$$

where $\Delta f_{\pm 3dB}$ is the 3 dB-bandwidth, f_H represents higher resonant frequency, and f_L denotes lower resonant frequency.

Figure 3A,B show the $Q_{eS,eL}$ values determined via EM simulation of QM and OEM SIW cavities. $Q_{eS,eL}$ can be controlled by moving the tap position from the short circuit of the via-hole. The $Q_{eS,eL}$ value of QM and OEM SIW cavities decreases as the tap distances from the via-hole ($L_{1,2}$) increase. The extracted K_{12} value of QM/QM SIW cavities is presented in Figure 3C, and the K_{23} value of QM/OEM SIW cavities is shown in Figure 3D. The values of K_{12} and K_{23} rise as the width of iris windows W_1 and W_2 increases. The bandwidth (BW) of the SIW BPF was controllable by adjusting the coupling iris window.

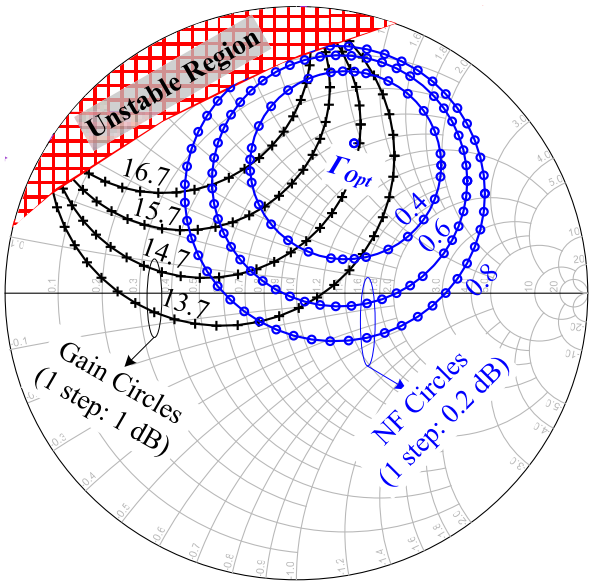

FIGURE 4 Simulated gain and NF circles of CE3512 from CEL

3 | LNAS DESIGN

3.1 | CLNA designs

Three LNAs with different IMNs were designed using CE3512K2 from California Eastern Laboratories (CEL), and we compared their electrical performance and circuit size. Figure 4 displays simulated gain and noise figure (NF) circles which were generated using advanced design systems (ADS) software. Under the bias conditions of

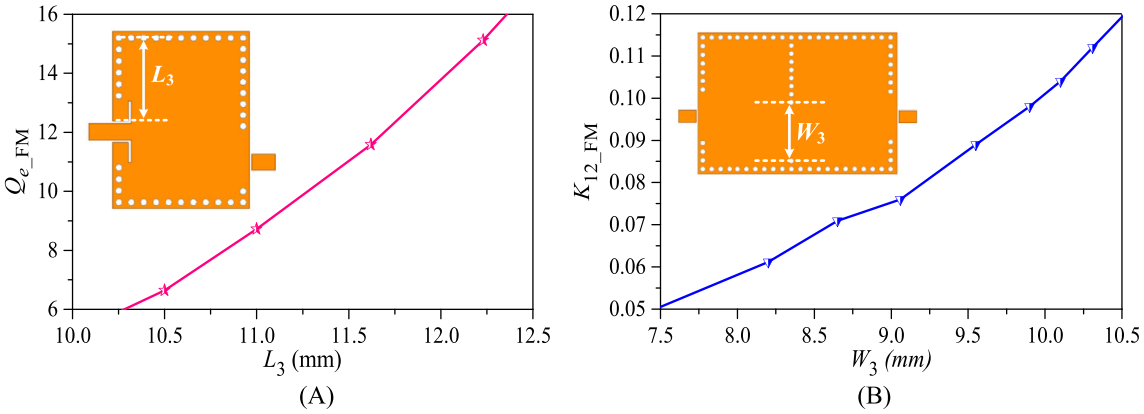

FIGURE 5 (A) $Q_{eS,eL}$ of an FM SIW cavity according to L_3 and (B) K_{12} of two FM SIW cavities according to W_3

$V_{DS} = 2$ V and $I_{DS} = 10$ mA, input (Z_S) and output (Z_L) impedances at $f_0 = 8$ GHz were selected as $27.5 + j25\ \Omega$ and $28.5 + j15\ \Omega$, respectively. By terminating the impedances at the S2P file of CE3512K2, and performing the simulation using ADS software, a small-signal gain of 15.8 dB and an NF of 0.58 dB were observed. The CLNA was designed with conventional matching networks using open stubs and series MLs.

3.2 | Design of a CLNA with FM SIW BPF

Generally, BPFs and amplifiers are designed separately, as shown in Figure 1A. In this study, we design an FM SIW BPF with a termination impedance of 50-to-50 Ω, which was cascaded with a CLN. The FM SIW BPF was designed with the fractional bandwidth (FBW), passband ripple, and resonator order (n) of 10%, 0.0436, and 3, respectively. $Q_{eS} = Q_{eL} = 8.53$ was calculated using Equation (4), and $K_{12} = K_{23} = 0.103$ was calculated using Equation (5). Figure 5A shows the observed $Q_{eS,eL}$ value following EM simulation of an FM SIW cavity. The $Q_{eS,eL}$ value can be controlled by moving the tap distance (L_3) from the short circuit of the via-hole. The $Q_{eS,eL}$ of an FM SIW cavity rise as the tap distance (L_3) increases.

The K_{12_FM} value of two FM SIW cavities is presented in Figure 5B. The value of K_{12_FM} rises as the width of the iris window W_3 increases. Since a 50-to-50 Ω BPF is followed by a CLNA, the overall NF can be calculated using Friis equation and can be represented as $NF_{total} = NF_{50\Omega\ BPF} + NF_{CLNA}$, where $NF_{50\Omega\ BPF}$ is the NF of FM SIW BPF and NF_{CLNA} is the NF of CLNA.[1] If the FM SIW BPF and CLNA are not perfectly matched to 50 Ω, or they are not well-cascaded to each other, the observed NF_{total} may be different from the ideal value.

3.3 | Co-design of an LNA with compact SIW BPF IMN

In the co-design process, a compact SIW BPF was designed directly to match the Z_S of LNT. Therefore, the issues mentioned in the previous subsection can be omitted from the design consideration. A compact SIW BPF was designed to replace the IMN of a CLNA, while the output matching network remained identical. The compact SIW BPF IMN was designed for arbitrary termination impedances and was not limited to 50-to-50 Ω. Since the SIW BPF was grounded with via-holes, the bias circuits for the LNT with a dc-block had to be as small as possible. The termination impedance of the compact SIW BPF IMN was configured as a complex termination impedance (CTI) of Z_{in} of LNT and 50 Ω of antenna. Electrical simulation with ADS software resulted in $Z_{in} = 81.5 + j48.5\ \Omega$. The process to observe Z_{in} was briefly denoted in Figure 6. The SIW BPF IMN proposed in this study utilizes QM and OEM SIW cavities. The first and second stages are consistent with the QM SIW cavities while the third stage is consistent with the OEM SIW cavity. From Equation (1), f_{L3} was calculated and detuned to 8.2838 GHz. Following the same approach described in Reference 5, $K_{12} = 0.0626$ and $K_{23} = 0.0553$ were observed. Similarly, $Q_{eS} = Q_{eL} = 8.53$ was determined using Equation (4). Since the first and second stages were realized from QM SIW cavities with an input termination impedance of 50 Ω, f_{r_QM} was equal to f_0. As the third stage resonator would be realized from OEM SIW cavity with an output termination impedance of Z_{in}, f_{r_OEM} was equal to f_{L3}. A Taconic TLY printed circuit board (PCB) with $\varepsilon_r = 2.2$ and $h = 0.508$ mm was used in this design. Finally, the edge lengths of the QM and OEM SIW cavities could be estimated using Equations (2) and (3).

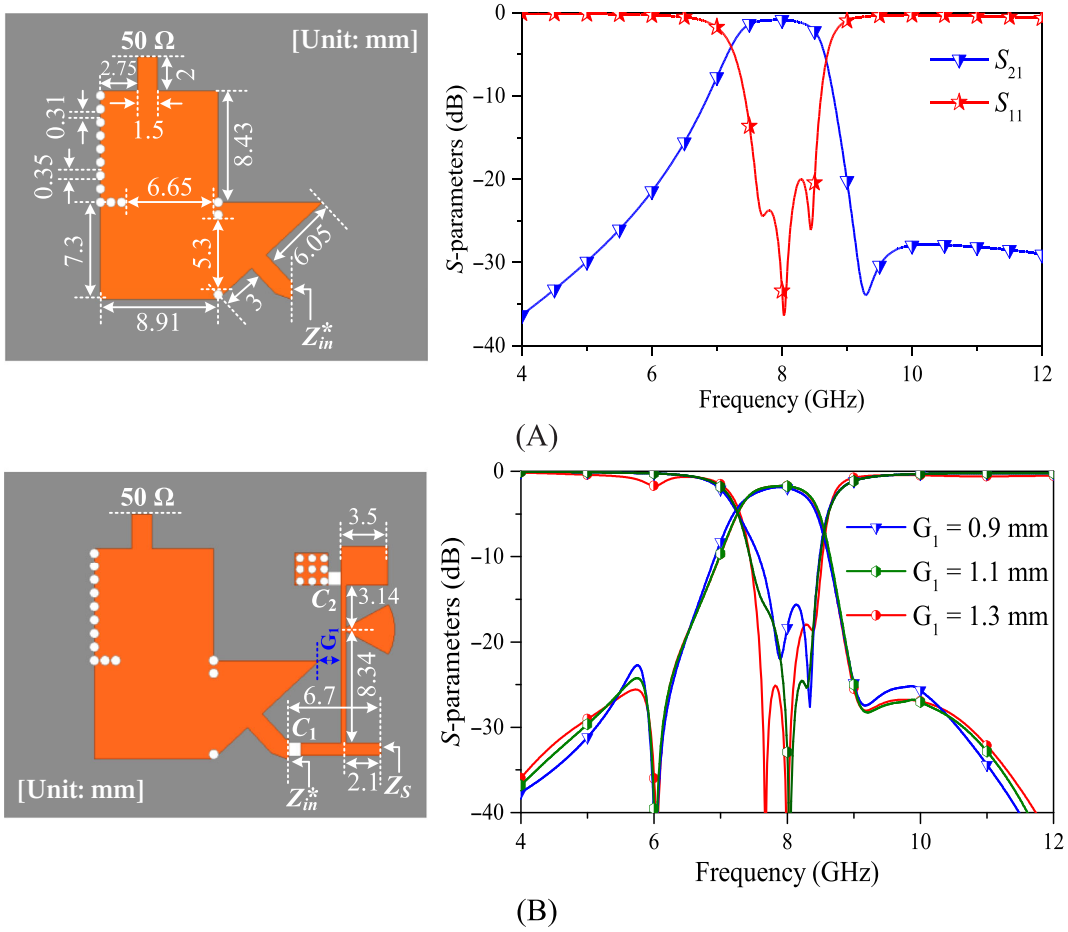

FIGURE 6 Layouts and frequency responses of (A) compact SIW BPF IMN, and (B) the circuit displayed in (A) connected to a bias circuit and DC-blocked capacitor according to G_1

4 | SIMULATION AND MEASUREMENT RESULTS

The compact SIW BPF IMN is located at the input part of the proposed LNA. The SIW BPF IMN is connected to the bias circuit at the gate terminal of the LNT. As mentioned in Reference 21, TZs may occur in mixed-mode SIW BPF due to small cross-coupling between the source and load. Figure 6 shows the layout and frequency response of the proposed SIW BPF IMN with real-to-complex termination impedances that were obtained via EM simulation. The input taper line of the proposed SIW BPF IMN is utilized as an impedance transformation between QM SIW cavities and the 50 Ω termination port. Similarly, the output taper line is utilized as the impedance transformer between the OEM SIW cavity and Z_{in}. The taper lines are utilized for matching purposes. As shown in Figure 6A, a TZ occurs at the higher side of the stopband. Moreover, when the circuit in Figure 6A is connected to the bias circuit, unwanted coupling between these circuits occurs. Due to this unwanted coupling, another TZ occurs at the lower side of the stopband as shown in Figure 6B. As a result, the TZs improved the frequency selectivity of the proposed compact SIW BPF IMN. We observed that the filtering response and the return losses of the proposed SIW BPF IMN deteriorate when the gap (G_1) between the OEM SIW cavity and the bias circuit becomes smaller. Figure 7A,B presents the matching impedance point comparison between the EM simulation and observed measurement results, as well as the *S*-parameter responses of the proposed SIW BPF IMN. The target source impedance is obtained at f_0 with a measured insertion loss of 0.9 dB. The BW of the fabricated IMN was narrower than the BW obtained from the EM simulation due to the slight tolerances in the fabrication process. The tolerances of the diameter of via-hole and the pitch between adjacent via-holes may cause a slightly changing to $K_{i,i+1}$ of SIW cavities. As the $K_{i,i+1}$ was slightly different from the target value, the filtering response, return losses, and BW of the SIW BPF are deteriorated.

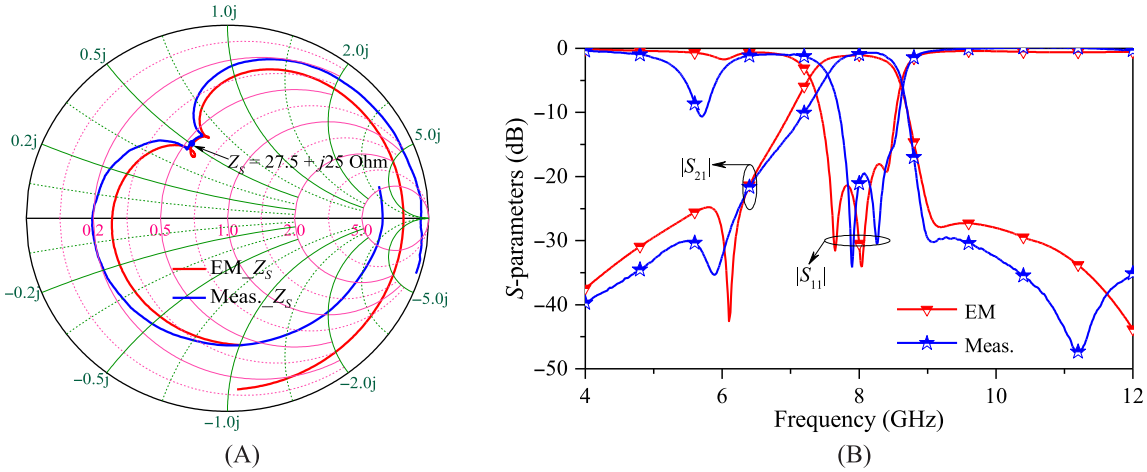

FIGURE 7 Comparison between EM simulation and measurement results of the proposed SIW BPF IMN (A) matching impedance points and (B) *S*-parameter responses

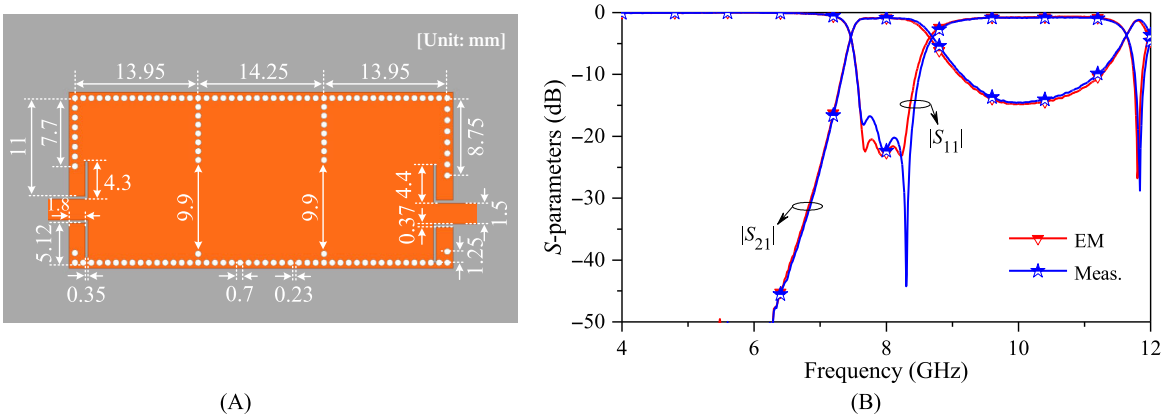

FIGURE 8 FM SIW BPF with 50-to-50 Ω termination impedances (A) layout and (B) *S*-parameter responses

The layout and frequency responses of the FM SIW BPF with a 50-to-50 Ω termination impedance are shown in Figure 8A,B. At f_0, the insertion loss of FM SIW BPF is 0.89 dB. The measurement results are consistent with the results obtained from the EM simulation. The attenuation level was superb on the lower side of the stopband, but poor on the higher side.

Photographs of the fabricated LNAs are shown in Figure 9. In this experiment, the FM SIW BPF was cascaded with a CLNA via a high-*Q* chip capacitor which had a capacitance of approximately 3.67 pF at f_0. The use of QM and OEM SIW cavities as the IMN produced an LNA with a 48% smaller circuit size than the FM SIW BPF cascaded with a CLNA.

Figure 10A shows the measured *S*-parameters of three LNAs within the frequency range of 4 to 12 GHz. We found that the small-signal gains at f_0 of the proposed LNA, CLNA, and FM SIW BPF cascaded with CLNA are 15.18, 15.69, and 14.72 dB, respectively. Even though the CLNA demonstrates the highest small-signal gain, a receiving BPF is required for interferer suppression. The proposed LNA demonstrates a minimum attenuation of 25.4 dB between 4 and 6.64 GHz, and 27.3 dB between 8.74 and 12 GHz. According to the filtering responses of the designed SIW BPF IMN, the proposed LNA provides better attenuation than the FM SIW BPF cascaded with CLNA at the higher side of the stopband.

The comparison of measured NFs is shown in Figure 10B. At f_0, we observed that the measured NFs of the proposed LNA, CLNA, and the FM SIW BPF cascaded with CLNA are 1.71, 0.86, and 2.13 dB, respectively. The proposed LNA provides a lower NF than FM SIW BPF cascaded with CLNA. Figure 11A shows the 1 dB compression point (P_{1dB}) and gain of the fabricated LNAs according to the input power (P_{in}) level. At f_0, we denoted that the measured P_{1dB} of the proposed LNA is 9.17 dBm, CLNA is 9.36 dBm, and FM SIW BPF cascaded with CLNA is 9.01 dBm. At P_{1dB}, the gain of the proposed LNA is 14.1 dB, CLNA is 14.54 dB, and FM SIW BPF cascaded with CLNA is 13.74 dB. The IIP3 and OIP3 of the

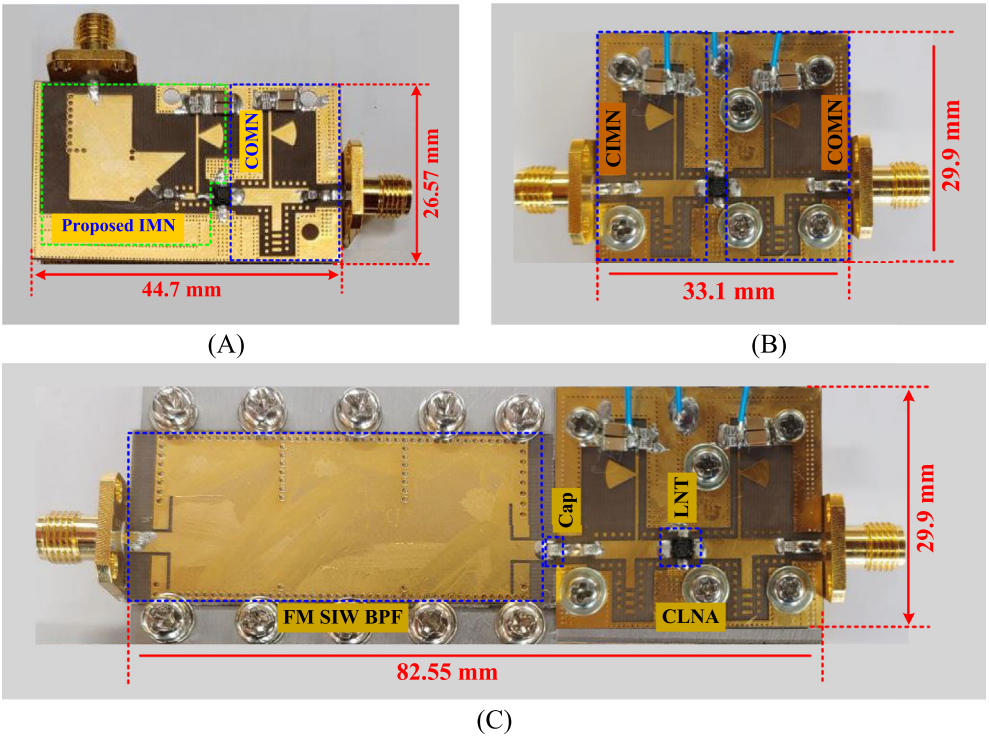

FIGURE 9 Photographs of fabricated LNAs (A) proposed LNA, (B) CLNA, and (C) FM SIW BPF cascaded with CLNA

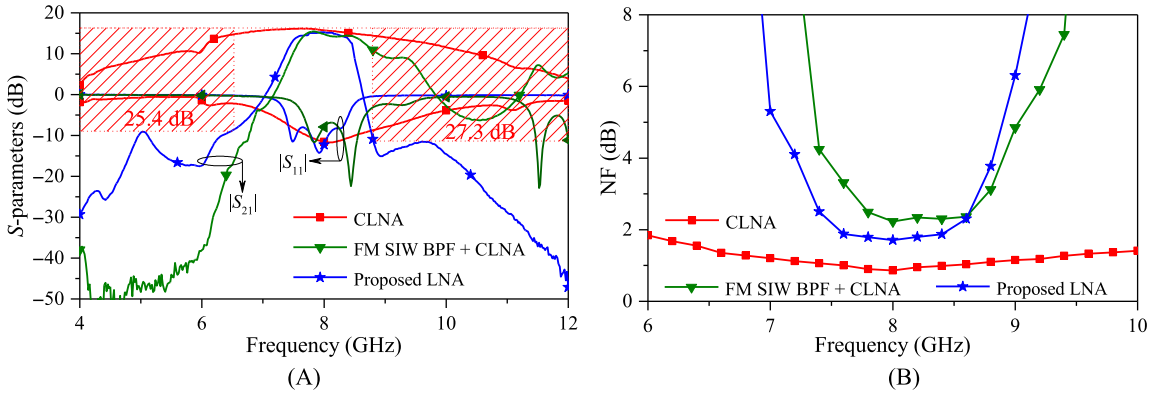

FIGURE 10 Comparison of (A) *S*-parameters and (B) NFs measurements

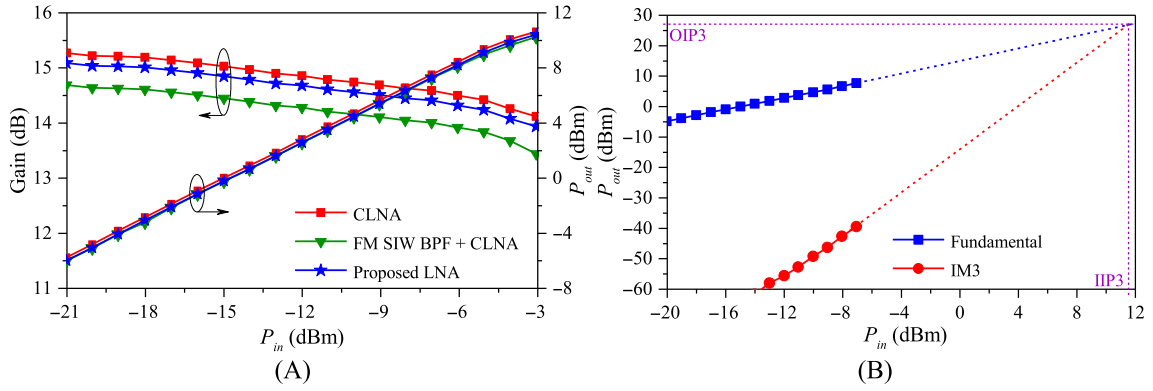

FIGURE 11 (A) measured P_{out} and gain of the fabricated LNAs, and (B) measured IIP3 and OIP3 of the proposed LNA

TABLE 1 Comparison of measurement results at f_0

	P_{1dB} (dBm)	Gain (dB)	NF (dB)	Size ($\lambda_0 \times \lambda_0$)
CLNA	9.36	15.69	0.86	$0.88\lambda_0 \times 0.79\lambda_0$
FM SIW BPF with CLNA	9.01	14.72	2.23	$2.20\lambda_0 \times 0.79\lambda_0$
Proposed LNA	9.17	15.18	1.71	$1.19\lambda_0 \times 0.70\lambda_0$

TABLE 2 Electrical performances comparison between proposed LNA and state-of-the-art amplifiers

	f_0 (GHz)	FBW (%)	P_{out} (dBm)	NF (dB)	Gain (dB)	MNs	n	TZs	Size ($\lambda_0 \times \lambda_0$)	Trans. type
2	10	5	6.8	N/A	12	Waveguide BPF	2	No	$2.66\lambda_0 \times 1.66\lambda_0$	HJ FET (low noise)
3	10	5	NA	N/A	11.1	Waveguide BPF	2	No	$4.16\lambda_0 \times 1.66\lambda_0$	HJ FET (low noise)
4	10	5	5.55	3	9	FM SIW BPF	2	No	$2.55\lambda_0 \times 0.95\lambda_0$	HJ FET (low noise)
5	10	5	35.42	N/A	5.49	FM SIW BPF	3	No	$2.61\lambda_0 \times 1.4\lambda_0$	GaN HEMT (power)
24	2.5	2	N/A	N/A	14	Capacitive SIW	N/A	No	$2\lambda_0 \times 0.5\lambda_0$	SiGe (low noise)
25	0.9	22.5	41.5	N/A	11.7	SISL BPF	2	Yes	$0.12\lambda_0 \times 0.07\lambda_0$	MOSFET (power)
26	5.5	3.6	38.5	N/A	12.5	SIW BPF Balun	2	Yes	$3.45\lambda_0 \times 2.88\lambda_0$	GaAs (power)
This work	8	10	9.17	1.71	15.18	QM and OEM SIW BPF	3	Yes	$1.19\lambda_0 \times 0.7\lambda_0$	FET (low noise)

proposed LNA are shown in Figure 11B. The IIP3 is around 11.8 dBm and the OIP3 is ~27 dBm. The electrical performance and circuit sizes of the fabricated LNAs are summarized in Table 1.

The performance of the proposed LNA and state-of-the-art amplifiers are compared in Table 2. In References 2, 3, the BPF MNs were fabricated using coupled waveguide cavities with very high Q-factors. However, the fabrication and the waveguide-to-ML transition would be difficult. In References 4, 5, the BPF MNs were constructed using FM SIW cavities that occupied large areas on the circuit board. In Reference 24, the amplifier was designed using capacitive SIW MNs, but the filtering response was not considered. In Reference 25, the amplifier was designed using metal integrated and substrate-integrated suspended lines (MI-SISL). The BPF MNs were implemented using SISL-based dual-layer interdigital capacitors and SISL-based dual-layer spiral inductors. The circuit size of that amplifier was very compact. In Reference 26, a BPF push-pull amplifier was utilized using a SIW balun power divider on two-layer PCB. However, the fabrication process and price would be difficult and costly for amplifiers in References 25, 26. Unlike the other works, the proposed amplifier used simple ML, QM, and OEM SIW cavities. The proposed amplifier was implemented on a single-layer PCB, which is an inexpensive design and easy to fabricate. In addition, the size of the proposed amplifier is compact compared to those state-of-the-art amplifiers, except for the amplifier in Reference 25.

5 | CONCLUSION

This article demonstrated a new co-design approach for SIW BPF and LNA using QM and OEM SIW cavities. For experimental demonstration, the proposed LNA and two other kinds of LNAs were fabricated. The electrical performance and circuit size of the three fabricated LNAs were compared with each other and state-of-the-art amplifiers. The proposed LNA provided the lower NF, possessed a much smaller circuit size compared to other filter amplifiers, and was capable of removing a receiving BPF. Thus, the overall size and complexity of the receiver in the RF front-end circuitry system can be relaxed using this concept. The results of the electrical performances comparison confirm that the proposed method can be applied to microwave circuits and systems designs. In addition, the proposed LNA can be used in radar systems.

ACKNOWLEDGMENTS

This work was supported by the National Research Foundation (NRF) of Korea Grant funded by Korea

Government (MSIT), under Grant 2020R1A2C2012057 and in part by Basic Science Research Program through the NRF of Korea, funded by Ministry of Education, under Grant 2019R1A6A1A09031717. The authors would like to thank the Writing Center at Jeonbuk National University for its skilled proofreading service.

DATA AVAILABILITY STATEMENT

The data that supports the findings of this study are available in the supplementary material of this article.

ORCID

Phanam Pech https://orcid.org/0000-0002-1443-5086
Yongchae Jeong https://orcid.org/0000-0001-8778-5776

REFERENCES

1. Razavi B. *RF Microelectronics*. 2nd ed. *Pearson Education, Inc.*; 2012:157-250.
2. Gao Y, Powell J, Shang X, Lancaster MJ. Coupling matrix-based design of waveguide filter amplifiers. *IEEE Trans Microw Theory Techn*. 2018;66(12):5300-5309.
3. Gao Y, Shang X, Guo C, Powell J, Wang Y, Lancaster MJ. Integrated waveguide filter amplifier using the coupling matrix technique. *IEEE Microw Wirel Compon Lett*. 2019;29(4):267-269.
4. Gao Y, Zhang F, Lv X, et al. Substrate integrated waveguide filter-amplifier design using active coupling matrix technique. *IEEE Trans Microw Theory Techn*. 2020;68(5):1706-1716.
5. Pech P, Kim P, Jeong Y. Microwave amplifier with substrate integrated waveguide bandpass filter matching network. *IEEE Microw Wirel Compon Lett*. 2021;31(4):401-404.
6. You CJ, Chen ZN, Zhu XW, Gong K. Single-layered SIW post-loaded electric coupling-enhanced structure and its filter application. *IEEE Trans Microw Theory Techn*. 2013;61(1):125-130.
7. Hao ZC, Ding WQ, Hong W. Developing low-cost W-band SIW bandpass filters using the commercially available printed-circuit-board technology. *IEEE Trans Microw Theory Techn*. 2016;64(6):1775-1786.
8. Chu P, Hong W, Tuo M, et al. Dual-mode substrate integrated waveguide filter with flexible response. *IEEE Trans Microw Theory Techn*. 2017;65(3):824-830.
9. Wang Y, Hong W, Dong Y, et al. Half mode substrate integrated waveguide (HMSIW) bandpass filter. *IEEE Microw Wirel Compon Lett*. 2007;17(4):265-267.
10. Cheng Y, Hong W, Wu K. Half mode substrate integrated waveguide (HMSIW) directional filter. *IEEE Microw Wirel Compon Lett*. 2007;17(7):504-506.
11. Lai Q, Fumeaux C, Hong W, Vahldieck R. Characterization of the propagation properties of half-mode substrate integrated waveguide. *IEEE Trans Microw Theory Techn*. 2009;57(8):1996-2004.
12. Camdoo R, Lau SM, Su HT. Compact cross-coupled half-mode substrate integrated waveguide bandpass filter. *Proc Asia Pasific Microw Confer (APMC)*. 2017;33:706-709.
13. Zhang ZY, Yang N, Wu K. 5-GHz bandpass filter demonstration using quarter-mode substrate integrated waveguide cavity for wireless system. *IEEE Radio Wireless Symp (RWS)*. IEEE; 2009:95-98.
14. Jin C, Shen Z. Compact triple-mode filter based on quarter-mode substrate integrated waveguide. *IEEE Trans Microw Theory Techn*. 2014;62(1):37-45.
15. Moscato S, Tomassoni C, Bozzi M, Perregirini L. Quarter-mode cavity filters in substrate integrated waveguide technology. *IEEE Trans Microw Theory Techn*. 2016;64(8):2538-2547.
16. He Z, You CJ, Leng S, Li X, Huang YM. Compact bandpass filter with high selectivity using quarter-mode substrate integrated waveguide and coplanar waveguide. *IEEE Microw Wirel Compon Lett*. 2017;27(9):809-811.
17. Xiangjun Z, Caoyuan M, Deqiang C. Compact dual-passband LTCC filter exploiting eighth-mode SIW and SIW hybrid with coplanar waveguide. *Electron Lett*. 2014;50(24):1849-1851.
18. Zhu Y. Design of a novel multi-layered eighth-mode substrate integrated waveguide filter by HFSS. *IEEE 6th International Symposium on Microwave, Antenna, Propagation, and EMC Technologies (MAPE)*. IEEE; 2015:620-622.
19. Li P, Chu H, Chen RS. Design of compact bandpass filter using quarter-mode and eighth-mode SIW cavities. *IEEE Trans Compon Packag Manuf Technol*. 2017;7(6):956-963.
20. Wang X, Zhu XW, Jiang ZH, Hao ZC, Wu YW, Hong W. Analysis of eighth-mode substrate-integrated waveguide cavity and flexible filter design. *IEEE Trans Microw Theory Techn*. 2019;67(7):2701-2711.
21. Kim P, Jeong Y. Compact and wide stopband substrate integrated waveguide bandpass filter using mixed quarter- and one-eighth modes cavities. *IEEE Microw Wirel Compon Lett*. 2020;30(1):16-19.
22. Swanson D, Macchiarella G. Microwave filter design by synthesis and optimization. *IEEE Microw Mag*. 2007;8(2):55-69.
23. Matthaei GL, Young L, Jones EMT. *Microwave Filter, Impedance-Matching Networks, and Coupling Structures*. McGraw-Hill; 1964.
24. Smith JN, Stander T. A capacitive SIW discontinuity for impedance matching. *IEEE Trans Compon Packag Manufact Techn*. 2019;9(11):2257-2266.
25. Feng T, Ma K, Wang Y, Hu J. Bandpass-filter power amplifier with compact size and wideband harmonic suppression. *IEEE Trans Microw Theory Techn*. 2022;70(2):1254-1268.
26. Feng W, Shi Y, Zhou XY, Shen X, Che W. A bandpass push-pull high power amplifier based on SIW filtering balun power divider. *IEEE Trans Plasma Sci*. 2019;47(9):4281-4286.

How to cite this article: Pech P, Kim P, Jeong Y. Co-design of a low noise amplifier with compact substrate integrated waveguide bandpass filtering matching network. *Int J RF Microw Comput Aided Eng*. 2022;e23498. doi:10.1002/mmce.23498